Analysis of Electrostatically Induced Interconnect Structures in Single-Layer Graphene via a Conservative First-Principles Modeling Technique

Emile Vanderstraeten and Dries Vande Ginste
quest, IDLab, Department of Information Technology, Ghent University/imec, Ghent, Belgium
emile.vanderstraeten@UGent.be, dries.vandeginste@UGent.be

***Abstract*—Electrostatically induced interconnect structures in graphene are an alluring alternative for nanoribbons to be used in future integrated circuits (ICs) because of the avoidance of edge scattering. In this contribution, these structures are analyzed using a novel first-principles modeling approach, based on higher-order conservative partitioned Runge-Kutta time stepping for the (2+1)D Dirac equation. The validity and applicability of the modeling tool are demonstrated by applying it to a bent interconnect and to a coupler.**

***Index Terms*—graphene, interconnect analysis, quantum mechanical modeling, conservative time stepping**

I. Introduction

The continuous downscaling of the IC feature size has been the main driving force behind the unceasing increase in performance of electronic devices. One of the main challenges resides in the design of high-quality interconnect structures as for smaller cross sections the resistance of Cu interconnects increases considerably. The resulting rise in RC-delay and power dissipation seriously restricts the performance of the IC.

Carbon nanotubes (CNT) and graphene nanoribbons (GNR) have been proposed as alternatives for Cu interconnects. These allotropes of carbon have a high current carrying capability, a long mean free path, due to reduced electron-phonon scattering, and there are no electromigration concerns [1]. Quasi-1D conducting channels can also be created in single-layer graphene by means of an electrostatic potential that confines the electrons in one direction [2]. With respect to GNRs this approach has the advantage that edge scattering is avoided and, compared to CNTs, its (semiconducting or metallic) properties are easier to control.

In this contribution, we study such electrostatically induced interconnects in single-layer graphene. Specifically, we focus on a bend in a single interconnect and on the coupler composed of two interconnects. To obtain reliable, accurate simulations, we resort to a novel, first-principles quantum mechanical modeling technique, based on higher-order partitioned Runge-Kutta (PRK) time stepping for the (2+1)D Dirac equation. It was theoretically shown in [3], [4] that this method exhibits excellent conservation properties, mitigating spurious dissipation, and thus allowing for long-time simulations. The method is extended and adapted in this work to analyze the aforementioned interconnect structures.

II. Conservative modeling technique

Electrons in graphene adhere to a linear dispersion relation (instead of a parabolic one) and their motion, here in the (x,y)-plane, is therefore accurately described by the following time-dependent Dirac equation:

$$i\hbar\frac{\partial}{\partial t}\Psi(x,y,t) = \left[v_F\left(\sigma_x p_x + \sigma_y p_y\right) + V(x,y)\right]\Psi(x,y,t), \tag{1}$$

with $\Psi = \left(\begin{smallmatrix} u \\ v \end{smallmatrix}\right)$ the two-component wavefunction (also known as the Dirac spinor), $\sigma_x = \left(\begin{smallmatrix} 0 & 1 \\ 1 & 0 \end{smallmatrix}\right)$ and $\sigma_y = \left(\begin{smallmatrix} 0 & -i \\ i & 0 \end{smallmatrix}\right)$ the Pauli spin matrices, and $p_x = -i\hbar\frac{\partial}{\partial x}$ and $p_y = -i\hbar\frac{\partial}{\partial y}$ represent the momentum operators. The Fermi velocity is given by $v_F = 10^6$ m/s, while the electrostatic potential energy $V(x,y)$, defining the interconnects, will be described in Section III. For this so-called (2+1)D Dirac equation the particle probability density is given by $\Psi^\dagger\Psi$. To discretize this equation, a staggered spatial grid is utilized. The simulation domain of size $L_x \times L_y$ is subdivided into $N_x \times N_y$ unit cells. Within each unit cell (i,j) of size $\Delta x \times \Delta y$, the component u is defined at two positions, $(i\Delta x, j\Delta y)$ and $((i+1/2)\Delta x, (j+1/2)\Delta y)$, and component v is defined at two positions: $((i+1/2)\Delta x, j\Delta y)$ and $(i\Delta x, (j+1/2)\Delta y)$. The associated values are stored in the vectors $\boldsymbol{u}_1$, $\boldsymbol{u}_2$, $\boldsymbol{v}_1$ and $\boldsymbol{v_2}$. We propose to approximate the spatial derivatives in (1) by fourth-order central differences and by splitting u and v into real and imaginary component, yielding

$$\frac{\mathrm{d}\boldsymbol{q}}{\mathrm{d}t} = K\boldsymbol{p}\ , \quad \frac{\mathrm{d}\boldsymbol{p}}{\mathrm{d}t} = -K^T\boldsymbol{q}, \tag{2}$$

with

$$\boldsymbol{q} = \begin{pmatrix} \mathrm{Im}(\boldsymbol{u}_1) \\ \mathrm{Re}(\boldsymbol{u}_2) \\ \mathrm{Re}(\boldsymbol{v}_1) \\ \mathrm{Im}(\boldsymbol{v}_2) \end{pmatrix}, \quad \boldsymbol{p} = \begin{pmatrix} \mathrm{Re}(\boldsymbol{u}_1) \\ \mathrm{Im}(\boldsymbol{u}_2) \\ \mathrm{Im}(\boldsymbol{v}_1) \\ \mathrm{Re}(\boldsymbol{v}_2) \end{pmatrix}, \tag{3}$$

and K is equal to

$$\begin{pmatrix} \frac{-V_{u_1}}{\hbar} & 0 & -v_F D_x \otimes I & v_F I \otimes D_y \\ 0 & \frac{V_{u_2}}{\hbar} & v_F I \otimes D_y^T & v_F D_x^T \otimes I \\ v_F D_x^T \otimes I & v_F I \otimes D_y & \frac{V_{v_1}}{\hbar} & 0 \\ v_F I \otimes D_y^T & -v_F D_x \otimes I & 0 & \frac{-V_{v_2}}{\hbar} \end{pmatrix}. \tag{4}$$

The Kronecker product is indicated by $\otimes$ in (4) and V_{u_1} is a matrix with on its diagonal the values of the potential

energy evaluated at the grid positions of $\boldsymbol{u}_1$; likewise V_{u_2}, V_{v_1} and V_{v_2} are obtained. The matrices D_x and D_y represent the discretized versions of the spatial derivatives. Owing to the specific form of (2) an explicit, symplectic PRK time integrator can be employed [5]. Stepping in time from $t = n\Delta t$ to $t = (n+1)\Delta t$ corresponds to

$$\begin{array}{ll} \boldsymbol{Q}^{n,0} = \boldsymbol{q}^n & \boldsymbol{P}^{n,1} = \boldsymbol{p}^n \\ \boldsymbol{Q}^{n,1} = \boldsymbol{Q}^{n,0} + \Delta t\, B_1\, K \boldsymbol{P}^{n,1} & \boldsymbol{P}^{n,2} = \boldsymbol{P}^{n,1} - \Delta t\, b_1\, K^T \boldsymbol{Q}^{n,1} \\ \boldsymbol{Q}^{n,2} = \boldsymbol{Q}^{n,1} + \Delta t\, B_2\, K \boldsymbol{P}^{n,2} & \boldsymbol{P}^{n,3} = \boldsymbol{P}^{n,2} - \Delta t\, b_2\, K^T \boldsymbol{Q}^{n,2} \\ \vdots \quad , & \vdots \quad , \\ \boldsymbol{Q}^{n,s} = \boldsymbol{Q}^{n,s-1} + \Delta t\, B_s\, K \boldsymbol{P}^{n,s} & \boldsymbol{P}^{n,s+1} = \boldsymbol{P}^{n,s} - \Delta t\, b_s\, K^T \boldsymbol{Q}^{n,s} \\ \boldsymbol{q}^{n+1} = \boldsymbol{Q}^{n,s} & \boldsymbol{p}^{n+1} = \boldsymbol{P}^{n,s+1} \end{array} \tag{5}$$

where the intermediate values are denoted by capital letters. The constants b_i and B_i, where i ranges from 1 to s, the number of substeps, characterize the PRK method. In this contribution, a fourth-order method is employed. Note that (2) is a Poisson system, and thus it can be shown that the advocated PRK time stepping method conserves the energy and the particle probability density, this in contrast to methods based on standard explicit RK time stepping [3]. These conservation properties allow for long-time simulations, needed for accurate interconnect analysis.

III. Analysis of Interconnect Structures

A. Simulation setup

The simulation setup for the interconnect structures under study is depicted in Fig. 1. To account for open boundaries, the simulation domain is terminated by an absorbing layer of thickness t_{AB} [6]. The interconnects are constructed by means of a confining potential that has the form of a hyperbolic secant potential [2]. For example, for a section along the y-dimension this potential is given by

$$V(x,y) = -\frac{V_0}{\cosh(\beta x)}, \tag{6}$$

with $\beta = \frac{2\,\text{arccosh}(2)}{W}$ and W the full width at half maximum. In practice, this potential profile can be realized approximately by means of a wire suspended above a graphene plane [2], [7]. As value for W, 8 nm was employed, which — according to [7] — is a realistic value. The parameter V_0 equals 0.25 eV. At the orange line, an electron with energy E is injected into the interconnect; this particle is represented by a wave packet with time dependency $e^{-iEt/\hbar}$ which is further modulated by an additional Gaussian $1/\sqrt{2\pi\sigma_t}\; e^{(t-t_0)^2/(2\sigma_t)^2}$, with σ_t and t_0 determining the width and the position of the Gaussian, respectively. Consequently, the source has a finite support in the time domain. At the observers, designated by the red and/or the blue line in Fig. 1, the incoming wavefunction is transformed to the energy domain by means of a fast Fourier transform and the expansion coefficient with respect to the single bound mode is determined. This way, the transmission from the source to the observer(s) can be extracted as a function of the energy E.

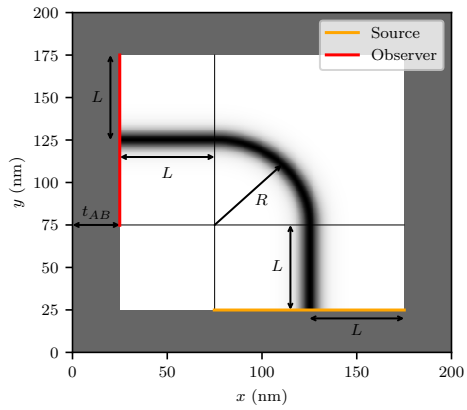

(a) Bend in a single interconnect

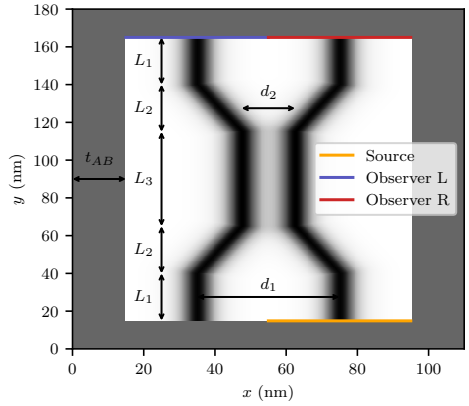

(b) Coupler composed of a pair of interconnects

Fig. 1: Interconnect structures in graphene: simulation setup

B. Bent interconnect: validation

For the simulation of the bent interconnect of Fig. 1a, the following values of the parameters are used: L=50 nm, $t_{\text{AB}} = 60$ nm, σ_t=80 fs and $t_0 = 480$ fs.. The radius of the bend R is varied between 10 nm and 50 nm. In Fig. 2 the transmission from source to observer is plotted. In the limit of large radius R, the bend losses disappear and the transmission equals one. This validates the advocated modeling approach, where clearly the particle density is conserved and no spurious dissipation is introduced.

C. Analysis of the coupler: application

For the simulation of the coupler, presented in Fig. 1b, the following values of the parameters are used: d_1=40 nm, L_1=15 nm, L_2=75 nm, $t_{\text{AB}} = 60$ nm, σ_t=80 fs and $t_0 = 480$ fs. The transmission from the bottom right source to the top left observer and to the top right observer as a function of the length of the coupling region L_3 are shown in Fig. 3. In the coupling region the distance between the interconnect d_2 equals 10 nm. Due to the coupling, part of the particle probability density is transferred from the right interconnect to the left one, while the other part is retained in the right one. Note that the transmission from right to left does not

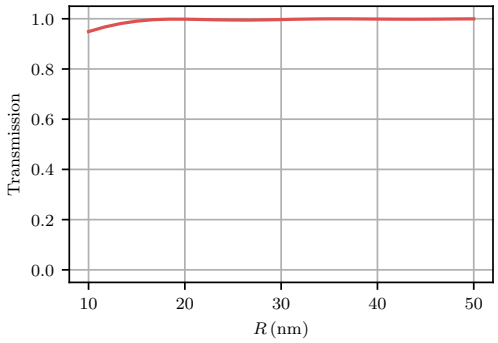

Fig. 2: Transmission through the bent interconnect from source to observer for an electron with energy value $E = 0$ as a function of the radius R.

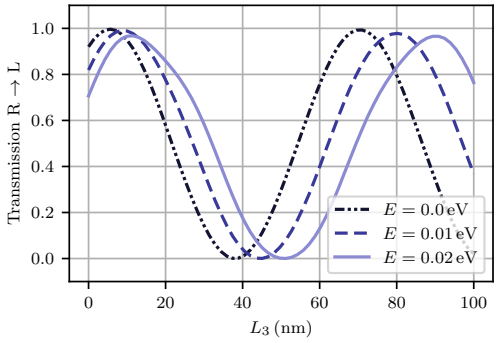

(a) Transmission from bottom right to top left.

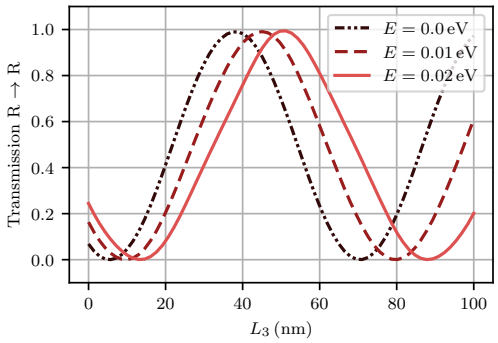

(b) Transmission from bottom right to top right.

Fig. 3: Transmission as a function of the length of the coupling region L_3 for three different values of the energy E.

go to zero for small values of L_3. This is explained by the fact that part of the coupling already occurs in the transition region of length L_2, thereby increasing the effective length of the coupling region. For larger values of the energy, the particle is better confined in the interconnect, which leads to less efficient coupling and a larger period.

In Fig. 4, d_2 is varied instead of the length L_3, which equals 100 nm in this case. Again, it is observed that the coupling strength is smaller for larger values of the energy. Furthermore, the coupling strength depends exponentially on the distance d_2.

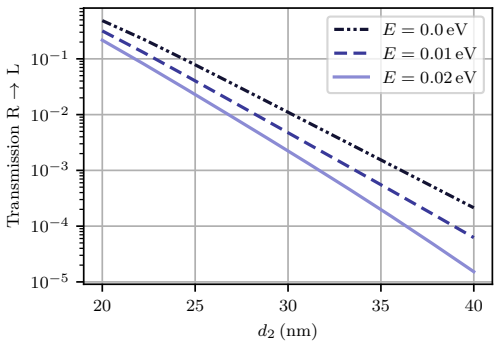

Fig. 4: Transmission from bottom right to upper left interconnect segment as a function of the distance between the interconnect in the coupling region d_2. The transmission is plotted for three different values of the energy E.

IV. Conclusion

In this work, we studied electrostatically induced interconnect structures in single-layer graphene for integration in future ICs. The analysis was performed using a novel first-principles modeling technique, based on conservative partitioned Runge-Kutta time stepping for the (2+1)D Dirac equation. The validity and applicability of the modeling approach are demonstrated through two cases: a single bent interconnect and a coupler composed of two interconnects. For the latter, the exchange of probability density between the interconnects was clearly observed and a parameter study displayed the tunability of the device.

Note that — upon acceptance of the paper — during the conference time-domain animations of the motion of the electrons in the graphene interconnects will be shown.

Acknowledgment

The authors would like to thank Research Foundation - Flanders (FWO) for supporting this research (1107321N).

References

[1] H. Li, C. Xu, N. Srivastava, and K. Banerjee, "Carbon Nanomaterials for Next-Generation Interconnects and Passives: Physics, Status, and Prospects," *IEEE Trans. Electron Devices*, vol. 56, pp. 1799–1821, 2009.

[2] R. R. Hartmann, N. J. Robinson, and M. E. Portnoi, "Smooth electron waveguides in graphene," *Phys. Rev. B*, vol. 81, 2010.

[3] E. Vanderstraeten and D. Vande Ginste, "A conservative fourth-order real space method for the (2+1)D Dirac equation," *J. Comput. Appl. Math.*, vol. 428, pp. 1–19, 2023.

[4] ——, "Analysis of Electronic Waveguide Bends in Graphene Subject to Dirac Point Fluctuations," in *IEEE 6th Int. Conf. Emerging Electronics (ICEE)*, 2022, pp. 1–4.

[5] J. M. Sanz-Serna and M. P. Calvo, *Numerical Hamiltonian Problems*, 1st ed. Chapman and Hall, 1994.

[6] O. Pinaud, "Absorbing layers for the Dirac equation," *J. Comput. Phys.*, vol. 289, pp. 169–180, 2015.

[7] A. Cheng, T. Taniguchi, K. Watanabe, P. Kim, and J. D. Pillet, "Guiding Dirac Fermions in Graphene with a Carbon Nanotube," *Phys. Rev. Lett.*, vol. 123, 2019.